Journal of Materials Processing Technology 150 (2004) 255–262

Journal of Materials Processing Technology

www.elsevier.com/locate/jmatprotec

Microstructure and solidification thermal parameters in thin strip continuous casting of a stainless steel

J.E. Spinelli [a], J.P. Tosetti [b], C.A. Santos [a], J.A. Spim [c], A. Garcia [a,*]

[a] *Department of Materials Engineering, State University of Campinas, UNICAMP, P.O. Box 6122, 13083-970 Campinas, SP, Brazil*
[b] *Technology Research Institute, IPT, São Paulo, SP, Brazil*
[c] *Federal University of Rio Grande do Sul, UFRGS, Porto Alegre, RS, Brazil*

Received 12 November 2002; accepted 17 February 2004

Abstract

The present work focuses on the relationships between solidification thermal parameters and the dendritic microstructure of an AISI 304 stainless steel solidified both in a strip casting pilot equipment (twin-roll) and in a directional solidification simulator. Experimental studies were conducted with a stainless steel strip casting obtained in a twin-roll continuous caster pilot equipment and in samples solidified in a directional solidification simulator with two different melt superheats. In both cases, the surface of the substrates was similar, with mean surface roughness of about 0.3 μm. After solidification, the specimens were cut at different positions from the metal/mold interface and etched for metallographic examination. An empirical equation from the literature relating secondary dendrite arm spacing and cooling rates was used to demonstrate the similarity of the cooling efficiency. The results have shown that the simulator can be used in the determination of transient metal/mold interface coefficients (h_i) and in the preprogramming of the strip casting operational conditions as a function of roll materials and surface roughness.

Keywords: Twin-roll; Metal/mold heat transfer coefficient; Mathematical modeling; Microstructure

1. Introduction

During the early stages of solidification in near net shape processes, the total resistance to heat transfer from melt to the mold is mainly governed by the thermal resistance of the metal/mold interface, as opposed the conventional continuous casting, where the resistances of the solidifying shell and of the lubricant film are also significant [1,2]. In the twin-roll continuous casting operations, the molten metal is solidified directly on a substrate (two water cooled rolls) without a lubricant. The successful operation of the twin-roll machine depends strongly on the way in which sensible heat is extracted during the strip solidification [3–6].

The overall heat flow between metal and cooling water is affected by a series of thermal resistances, as shown in Fig. 1. Eq. (1) relates the overall metal/coolant heat transfer coefficient (h_i), with the metal/mold heat transfer coefficient ($h_{m/m}$) (which incorporates the gap formation), h_w, which is water/mold heat transfer coefficient and an equivalent heat transfer coefficient that takes into account the influence of mold wall thickness (k_m/e_m).

$$\frac{1}{h_i} = \frac{1}{h_w} + \frac{e_m}{k_m} + \frac{1}{h_{m/m}} \quad (1)$$

The interfacial thermal resistance between the mold and the solid metal shell (R_1) is generally the largest. In the absence of lubricant or coating, the surface roughness of the mold, and melt superheat may exercise a strong influence on the interfacial resistance, and consequently on the solidification microstructure.

Modeling of casting solidification can provide a method for improving casting yields. An accurate casting solidification model could be used to predict microstructure and to control the process based on thermal and operational parameters, and for this, it is necessary the previous knowledge of the transient metal/mold heat transfer coefficient.

Many investigations concerning the overall heat transfer coefficient between metal and mold have been carried out, and pointed out the importance of the development of appropriate tools to evaluate the heat transfer coefficient as a function of most of the variables of the casting processes [1–9]. Experimental works on heat transfer coefficients can only

* Corresponding author. Tel.: +55-19-3788-3320; fax: +55-19-3289-3722.
E-mail address: amaurig@fem.unicamp.br (A. Garcia).

0924-0136/$ – see front matter © 2004 Elsevier B.V. All rights reserved.
doi:10.1016/j.jmatprotec.2004.02.040

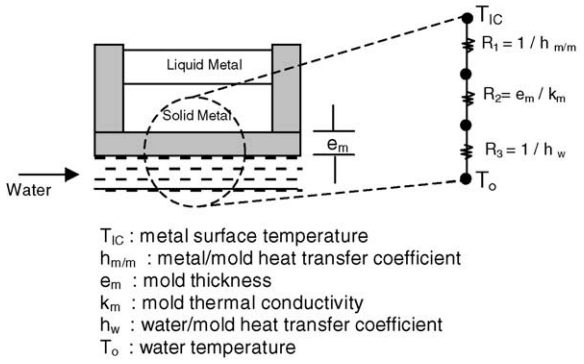

Fig. 1. Thermal resistances in a cooled metal/mold system.

produce values that are valid for the particular experimental conditions under which they are measured. In conventional continuous casting operations for slabs, blooms and billets, the as-cast microstructure is almost completely changed during reheating operations, but in strip casting processes, the as-cast structure is of major significance because, in most cases, the reheating stage is eliminated.

In the works by Strezov and co-workers [1–3], the initial stages of solidification of stainless steel samples onto a cold copper substrate were monitored to calculate the heat flux. The experimental apparatus was designed to approximate the initial contacting conditions of a twin-roll caster, by immersing a substrate into a furnace containing a 304 stainless steel melt. The substrates were instrumented with 0.25 mm diameter type-K thermocouples enabling the calculation of the interfacial heat flux over an area of several square millimeters with a millisecond resolution. The initial interfacial heat transfer was analyzed keeping constants: melt temperature, paddle immersion velocity and initial substrate temperature. The effects of the buildup and melting of oxide films such as manganese silicates at the interface, the substrate textures and the dynamic wetting phenomena, have also been analyzed.

Extensive results have been reported by Guthrie and co-workers [5,6] concerning the characterization of the instantaneous heat fluxes and heat transfer coefficients during the solidification of steel in a pilot scale 0.6 m diameter twin-roll caster, whose copper contact surfaces had been treated with coatings. The researchers used implanted thermocouples into the roll and the temperature data were acquired at a frequency of 2 and 10 Hz during the entire casting trials, which corresponded to approximately 250 s. The measured temperatures in the roll were then used in the solution of an inverse heat transfer problem to determine the interfacial heat fluxes. They have suggested that when thermocouples are used in the evaluation of transient heat fluxes by means of inverse methodologies, it is important to characterize the responses of the thermocouples so as to make any necessary adjustments in the temperature data for any estimate of the heat fluxes to be accurate. The apparatus and technique used in the temperature correction are described by Tavares [5], and involves plunging a thermocouple into a tapered hole set within a copper block of known temperature. Following the instant of contact, the temperature response curve for the thermocouple to reach the copper block temperature was logged and characterized using a transfer function based on the Laplace transform of process parameters. This procedure permits the correction of the temperature–time curves of the thermocouples for their thermal inertia. The resulting data are then used as input data for the inverse heat conduction program. The heat transfer coefficient, h_i, has generally been admitted to be constant along the strip/roll interface. This average was chosen through of the observed surface temperatures of strip and temperatures measured inside the rolls.

The present work focuses on the relationships between solidification thermal parameters and the dendritic microstructure of an AISI 304 stainless steel solidified both in a strip casting pilot equipment and in a directional solidification simulator.

1.1. Solidification mathematical model [10,11]

The development of model is based on the one-dimensional heat conduction equation, given by

$$\rho c \frac{\partial T}{\partial t} = \frac{\partial}{\partial x}\left[k(T)\frac{\partial T}{\partial x}\right] + \dot{q} \tag{2}$$

where ρ is the density (kg/m^3), c the specific heat (J/kg K), k the thermal conductivity (W/m K), $\partial T/\partial t$ the cooling rate (K/s), x the direction (m) and $\dot{q}$ is the heat source associated with phase change given by

$$\dot{q} = \rho L \frac{\partial f_s}{\partial t} \tag{3}$$

where f_s is the solid fraction during change phase (%) and L is the latent heat of fusion (J/kg).

The solid fraction depends on a number of parameters involved in the system. However, is quite reasonable to assume f_s varying only with temperature. The f_s can be obtained for stainless steel from, among other formulations [12].

Scheil's equation:

$$f_s = 1 - \left(\frac{T_f - T}{T_f - T_L}\right)^{1/(k_0 - 1)} \tag{4}$$

$$f_s \Rightarrow \begin{cases} 0, & T > T_L \\ 0 < f_s < 1, & \text{Scheil's equation} \\ 1, & T < T_S \end{cases} \tag{5}$$

where T_f is the fusion temperature (K), T_L the liquidus temperature and T_S is the solidus temperature, and by utilizing the concept of the pseudo-specific heat (c'), we obtain

$$c' = c - L\frac{\partial f_s}{\partial T} \tag{6}$$

and then we can substitute c from c' in Eq. (2).

The model also permits the insertion of physical properties as a function of temperature, considering the amount of solid as liquid fractions. At the range of temperatures, where solidification occurs for metallic alloys, the physical properties will be evaluated taking into account the amount of liquid and solid that coexists in equilibrium at each temperature given by

$$k = (k_S - k_L)\, f_s + k_L \tag{7}$$

$$c' = (c_S - c_L)\, f_s + c_L - L\, \mathrm{d}f_s \tag{8}$$

$$\rho = (\rho_S - \rho_L)\, f_s + \rho_L \tag{9}$$

where sub-indices S and L indicate, respectively, solid and liquid states. The final equations used by the solidification mathematical model are [10]:

$$T_i^{n+1} = \frac{\Delta t}{\tau_{i+1}} T_{i+1}^n + \frac{\Delta t}{\tau_{i-1}} T_{i-1}^n + \left(1 - \frac{\Delta t}{\tau_i}\right) T_i^n \tag{10}$$

where

$$\tau_{i+1} = C_{t_i}\, (R_{ti+1} + R_{ti}) \tag{11}$$

$$\tau_{i-1} = C_{ti}\, (R_{ti-1} + R_{ti}) \tag{12}$$

$$\frac{1}{\tau_i} = \frac{1}{\tau_{i+1}} + \frac{1}{\tau_{i-1}} \tag{13}$$

$$C_{ti} = \Delta x\, \Delta y\, \Delta z\, \rho c' \tag{14}$$

where $n+1$ is the index associated to the future time, n the index corresponding the actual time, Δt the increment in time (s), i the position, $\Delta x\, \Delta y\, \Delta z$ the nodal element volume (m^3) and C_{ti} is the thermal capacitance which represents the energy accumulated in a volume element i.

Eq. (10) becomes unstable for $\Delta t \leq \tau_{i,j}$ (stability limits). The thermal resistance at the heat flux line from point $i+1$ or $i-1$ to the point i is given by

$$R_{ti} = \frac{\Delta x_i}{k_i A_t}, \qquad R_{t_{i+1}} = \frac{\Delta x_{i+1}}{k_{i+1} A_t}, \qquad R_{t_{i-1}} = \frac{\Delta x_{i-1}}{k_{i-1} A_t} \tag{15}$$

For the mesh elements in contact with the rolls, the thermal resistance is given by

$$R_{t0} = \frac{1}{h_i A_t} \tag{16}$$

where h_i is the metal/coolant heat transfer coefficient ($W/m^2\,K$). More details of the overall mathematical model can be seen in previous articles [10,11,13].

1.2. Metal/mold heat transfer coefficient (h_i)

The method used to determine the metal/mold heat transfer coefficient is based on the solution of the inverse heat conduction problem (IHCP) [14–18]. This method makes a complete mathematical description of the physics of the process and is supported by temperatures measurements at known locations inside the heat conducting body. The temperature files containing the experimentally monitored temperatures are used in a finite difference heat flow model to determine h_i, as described in previous articles [8,9]. The process at each time step included the following: a suitable initial value of h_i is assumed and with this value, the temperature of each reference location in casting at the end of each time interval Δt is simulated by using an explicit finite difference technique. The correction in h_i at each interaction step is made by a value Δh_i, and new temperatures are estimated $T_{est}(h_i + \Delta h_i)$ or $T_{est}(h_i - \Delta h_i)$. With these values, sensitivity coefficients (ϕ) are calculated for each interaction given by

$$\phi = \frac{T_{est}(h_i + \Delta h_i) - T_{est}(h_i)}{\Delta h_i} \tag{17}$$

The procedure determines the value of h_i which minimizes an objective function defined by

$$F(h_i) = \sum_{i=1}^{n} (T_{est} - T_{exp})^2 \tag{18}$$

where T_{est} and T_{exp} are the estimated and the experimentally measured temperatures at various thermocouple locations and times, and n is the iteration stage. More details of the method for determination of h_i can be seen in a previous article [9].

2. Experimental procedure

The casting assembly used in solidification experiments is shown in Fig. 2. This experimental setup was designed to simulate the conditions of a twin-roll strip caster. Experiments were performed with an AISI 304 stainless steel, and a cooled steel chill was used, with the heat-extracting surface being polished. The thermophysical properties of the stainless steel are summarized in Table 1, as well as the casting conditions for the twin-roll pilot caster and the simulator. The water-cooling system used in the simulator was designed by adopting the same principles used in the pilot equipment. The internal geometry, pressure and flow characteristics were kept the same. The water inlet and outlet were monitored with 2.5 mm diameter type-K thermocouples, as indicated in Fig. 2.

The alloy was melted in an induction furnace until the molten metal reached a predetermined temperature (sample 1: 1620 °C; sample 2: 1760 °C), and then poured into the casting chamber (simulator and caster rolls). Temperatures in the simulator were monitored in the chill and in the casting during solidification via the output of type-S thermocouples (platinum–platinum 10% rhodium), 0.5 mm bead, accurately located with respect to the metal/mold interface.

All the thermocouples were connected by coaxial cables to a data logger interfaced with a computer, and the temperature data were acquired automatically. The chamber and the pilot

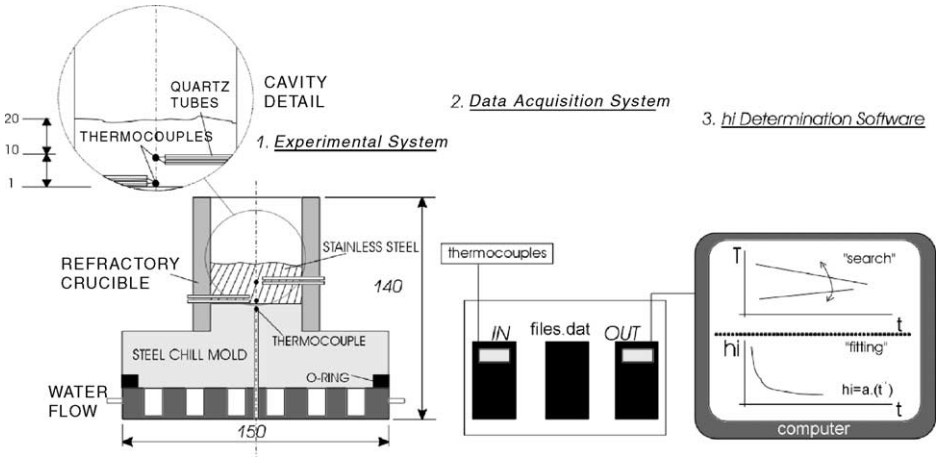

Fig. 2. Schematic representation of the unidirectional solidification assembly (mm).

equipment tundish were pre-heated by a heat blower and gas fire, respectively, and the molten metal surface after pouring was monitored using an optical pyrometer.

The chill surface was polished with grinding paper, and the surface roughness was determined by a digital system, where the arithmetic mean of the amplitude profile from the mean line (R_a in μm) was adopted to characterize the surface microgeometry. In all cases, the chill surface roughness was kept constant, with a mean value of about 0.30 μm.

After solidification, specimens were cut at different positions from the metal/mold interface and selected sections were polished and etched by an appropriate reagent (marble reagent: 20 g $CuSO_4$; 50 ml HCl; 50 ml H_2O) for metallographic examination [22]. Image processing systems Neophot 32 and Cambridge Leica-500 were used to measure secondary dendrite arm spacing (20 measurements for each selected position from the metal/mold interface).

3. Results and discussion

A typical thermal response obtained from the experiments in the directional solidification simulator is shown in Fig. 3 for thermocouples located in metal at 5 mm from the metal/mold interface and at 5 mm from the interface in the chill. The temperatures inside the molten metal de-

Table 1
Composition and thermophysical properties of metal and casting conditions

Composition balance being Fe	Thermophysical properties	
AISI 304 stainless steel [19–21]		
18.7 wt.% Cr	Thermal conductivity (solid) (W/m K)	31.0
9.1 wt.% Ni	Thermal conductivity (liquid)	30.3
0.08 wt.% C	Specific heat (solid) (J/kg K)	679
1.8 wt.% Mn	Specific heat (liquid)	670
1.3 wt.% Si	Density (solid) (kg/m^3)	7400
0.05 wt.% P	Density (liquid)	7600
0.02 wt.% S	Latent heat of fusion (J/kg)	260000
	Liquidus temperature (°C)	1460
	Solidus temperature	1399
	Partition coefficient	0.84
Parameters	Pilot equipment	Directional simulator
Casting conditions		
Mold material	Carbon steel	Carbon steel
Sample thickness	1–10 mm	15–20 mm
Surface roughness (R_a)	0.30 μm	0.30 μm
Pre-heating	600 °C	400–500 °C
Roll diameter	500 mm	–
Mold/chill thickness	50 mm	50 mm
Melt superheat	160 °C	160/300 °C
Protection gas	Argon	Argon
Mold/chill topography	Plane	Plane
Roll velocity	1 m/s	–

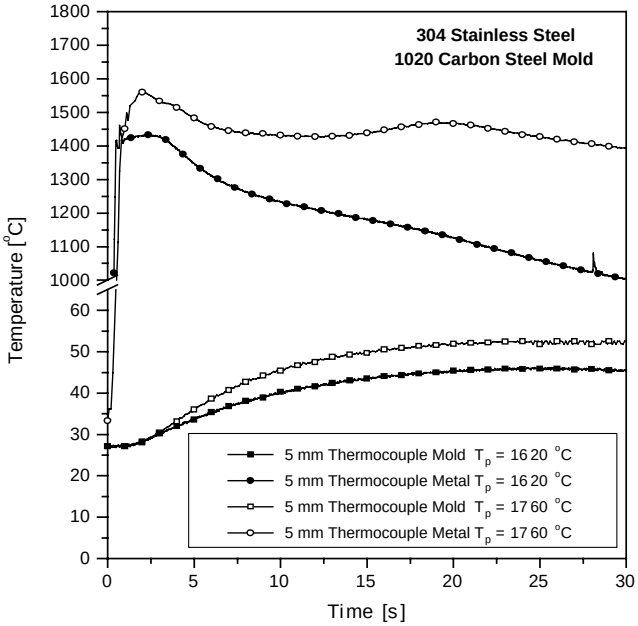

Fig. 3. Measured temperature responses for AISI 304 stainless steel: $T_p = 1620\,^{\circ}C$ and $1760\,^{\circ}C$ (melt superheat $\Delta T_p = T_p - T_L$).

crease with time, and the temperature at the chill increase very slowly once contact is established with the liquid metal until a constant value is attained, due the water cooling efficiency.

In these experiments, two different melt superheats (ΔT_p) were adopted: one close to that used for the molten metal in the pilot equipment during casting (160 °C) and other higher than the usual (300 °C), with the objective of analyzing the effect of this parameter on metal/mold heat transfer, and consequently, on the casting microstructure. The pouring time was about 3 s, which corresponds to the same value of the response time of the thermocouples (about 3–4 s). Temperature data were acquired at a frequency rate of 30 and 10 Hz for 160 and 300 °C melt superheats, respectively.

For both melt superheats a rapid solidification was observed to occur at 5 mm from metal/mold interface, about 5 and 30 s, respectively, demonstrating the efficiency of the cooling system. In this work, the correction of the response data of the thermocouples in the early times was made by using an immersion pyrometer to measure the molten metal temperature before pouring and an optical pyrometer to measure the liquid surface temperature into the cavity immediately after the complete pouring. These values were used as initial temperature input data for the mathematical model and the inverse method.

As observed in the caster pilot equipment, the inlet and outlet water temperatures can be considered constants with low variation for both cases. Fig. 4 shows these temperature data for 300 °C of melt superheat.

The dominant factor controlling overall heat transfer coefficient in the early stages of the process (before 5 s)

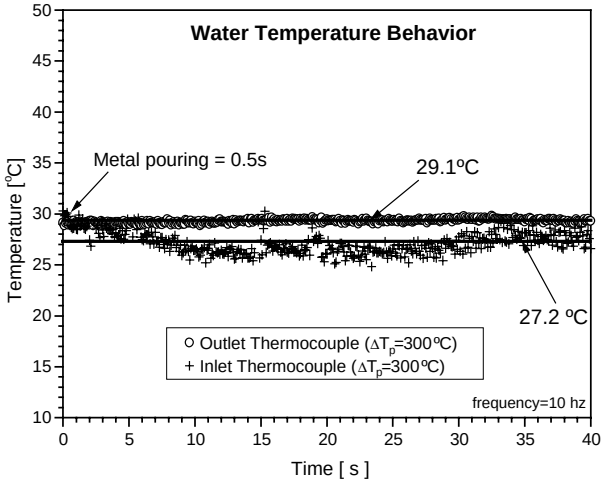

Fig. 4. Inlet and outlet water temperature responses: $\Delta T_p = 300\,^{\circ}C$.

includes the wettability of the mold surface by the melt, the type of material and mold surface roughness, the mold and metal thermophysical properties and initial temperatures. In this initial period, the solidifying shell contracts and the chill surface may expand, forming an interfacial gap. This extra thermal resistance introduced by gap accounts for the decrease in interfacial heat transfer coefficient, until an essentially constant behavior is attained where the casting shrinkage and the chill expansion do not have significant influences.

Figs. 5 and 6 show the best fit between experimental and simulated thermal responses and the corresponding metal/coolant interfacial heat transfer coefficients expressed as a power function of time.

The measured temperature in metal at 10 mm from the metal/mold interface was used as an initial boundary

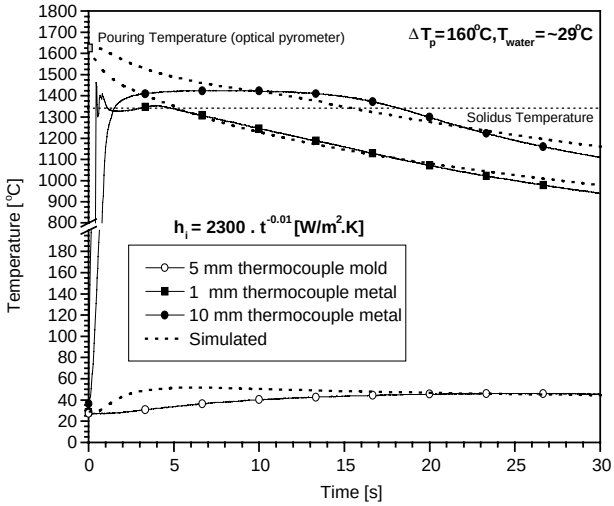

Fig. 5. Simulated and measured temperature responses in metal at 1 and 10 mm from the metal/mold interface as well as at 5 mm in the mold: $T_p = 1620\,^{\circ}C$.

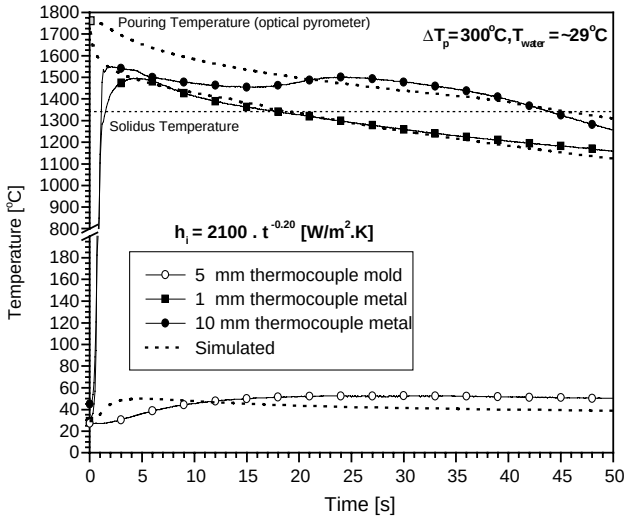

Fig. 6. Simulated and measured temperature responses in metal at 1 and 10 mm from the metal/mold interface as well as at 5 mm in the mold: $T_p = 1760^\circ C$.

condition while the thermocouple reading at 5 mm in the chill was used as an interior mold temperature, as well as the measured inlet water temperature in the cooling system. As can be observed in Figs. 5 and 6, in the early times (<5 s), the thermocouple responses were very slow, and the measured temperatures were below that corresponding to the pouring temperature that was measured utilizing an optical pyrometer during pouring.

Fig. 7 shows a comparison between the metal/mold heat transfer coefficients for both cases. It can be seen that for 300 °C of melt superheat, the initial h_i values are higher than those corresponding to $\Delta T_p = 160^\circ C$. The heat transfer coefficient increases with increasing values of superheat due the fluidity of molten alloys which increases with increasing temperature, favoring the wetting of the chill by the melt [8,16,21]. At the same time, the metallostatic pressure over the thin solidified shell is high due to the liquid metal weight.

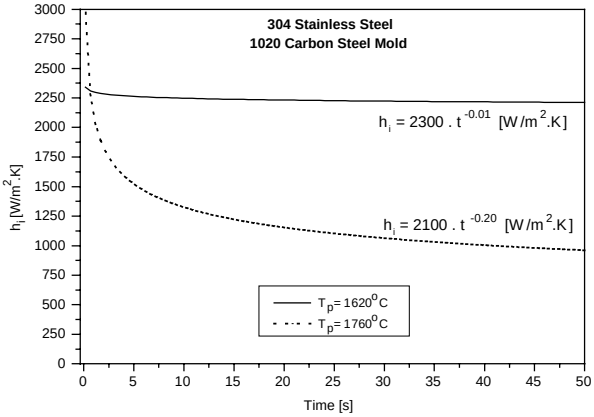

Fig. 7. Behavior of the metal/coolant heat transfer coefficient for the two experimental cases.

About 2 s later, this behavior changes, i.e. the h_i profile corresponding to the higher melt superheat is lower than that observed for the lower ΔT_p. As heat is extracted from the metal, the solidified shell becomes thicker and strong enough to support the metallostatic pressure, and h_i becomes approximately constant, as shown in Fig. 7. This is typical of the vertical physical configuration of the simulator, as discussed in a recent article [23]. However, considering the relatively low values of melt superheat normally used in the twin-roll casting operations it is expected that $h_i = 2300t^{-0.01}$ will best generate the experimental h_i profile for a 304 stainless steel solidified against steel rolls with a mean surface roughness of about 0.30 μm.

The solidification microstructures of castings produced in the simulator were predominantly columnar dendritic, with a dendritic array sufficiently defined to make possible accurate measurements, except at distances very near to the metal surface (<100 μm). Fig. 8a shows the dendrite morphologies from casting surface up to a position located at 800 μm inside the casting. The light etched area is γ phase and the dark area is δ ferrite phase, classified as skeletal, due to the high cooling rates. A typical solidification microstructure produced in the twin-roll strip casting pilot equipment is shown in Fig. 8b.

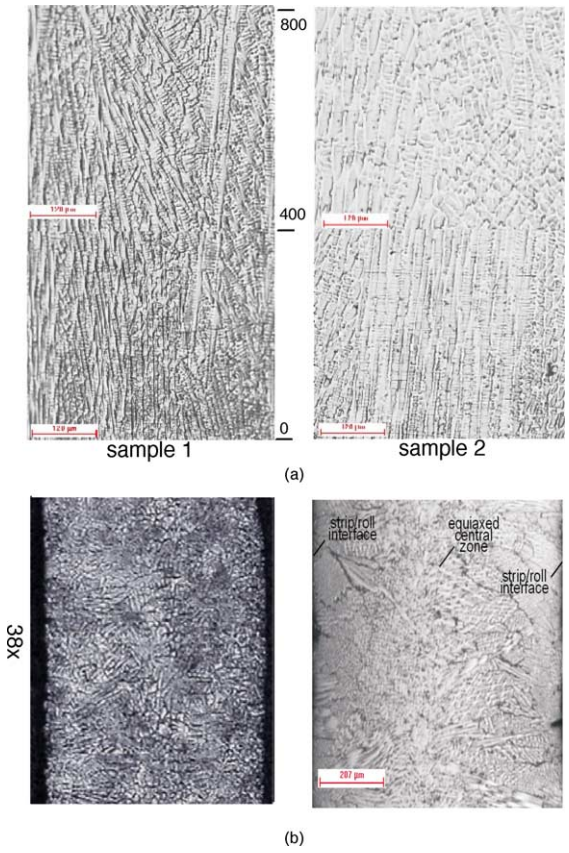

Fig. 8. (a) Experimental solidification microstructures of 304 stainless steel castings at different melt superheats: (sample 1) 160 °C, (sample 2) 300 °C; (b) longitudinal section: AISI 304 stainless steel strip casting.

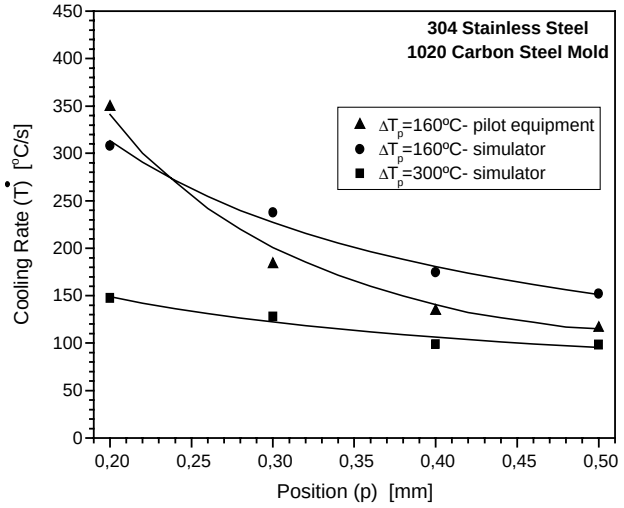

Fig. 9. Cooling rates calculated for the experimental casting and strip casting.

An experimental law from the literature [24] relating secondary dendritic spacings (λ_2 in μm) with cooling rates ($\dot{T}$ in K/s) during solidification of a 304 stainless steel is given by

$$\lambda_2 = 68\dot{T}^{-0.45} \quad (19)$$

Eq. (19) can be used to derive the cooling rates along solidification from the experimental measurements of λ_2, as shown in Fig. 9.

The resulting cooling rates during solidification in the simulator and those obtained for the strip casting pilot equipment, are quite similar for the same melt superheat, demonstrating that the simulator can be an useful tool in the planning of operational conditions of the strip casting equipment.

4. Conclusions

The similarity of thermal characteristics along solidification between the simulator and the pilot equipment observed in the present study enables the simulator to be used to gain insight into the strip casting process, by preprogramming strip casting operational conditions in terms of roll materials and surface roughness, and in the determination of the transient metal/coolant heat transfer coefficients which are fundamental for the mathematical simulation of solidification and control of the strip casting process.

Acknowledgements

The authors acknowledge financial support provided by FAPESP (The Scientific Research Foundation of the State of São Paulo, Brazil) and CNPq (The Brazilian Research Council). The authors are also grateful for the use of laboratory facilities at IPT (Technology Research Institute, SP, Brazil).

References

[1] L. Strezov, J. Herbertson, Experimental studies of interfacial heat transfer and initial solidification pertinent to strip casting, Iron Steel Inst. Jpn. Int. 38 (9) (1998) 959–966.
[2] L. Strezov, J. Herbertson, G. Belton, Mechanisms of initial melt/substrate heat transfer pertinent to strip casting, Metall. Trans. B 31 (10) (2000) 1023–1030.
[3] T. Evans, L. Strezov, Interfacial heat transfer and nucleation of steel-on-metallic substrates, Metall. Trans. B 31 (10) (2000) 1081–1089.
[4] R. Kopp, F. Hagemann, L. Hentschel, J. Schmitz, D. Senk, Thin-strip casting—modelling of the combined casting/metal-forming process, J. Mater. Proc. Technol. 80–81 (1998) 458–462.
[5] R. Tavares, M. Isac, R.I.L. Guthrie, Roll-strip interfacial heat fluxes in twin-roll casting of low-carbon steels and their effects on strip microstructure, Iron Steel Inst. Int. 38 (12) (1998) 1353–1361.
[6] R.I.L. Guthrie, M. Isac, J. Kim, R.P. Tavares, Measurements, simulations, and analyses of instantaneous heat fluxes from solidifying steels to the surfaces of twin roll casters and of aluminum to plasma-coated metal substrates, Metall. Trans. B 31 (10) (2000) 1031–1047.
[7] M. Martorano, J. Capocchi, Effects of processing variables on the microsegregation of directionally cast samples, Metall. Trans. A 31 (12) (2000) 3137–3147.
[8] J. Quaresma, C.A. Santos, A. Garcia, Correlation between unsteady-state solidification conditions, dendrite spacings, and mechanical properties of Al–Cu alloys, Metall. Trans. A 31 (12) (2000) 3167–3178.
[9] C.A. Santos, J. Quaresma, A. Garcia, Determination of transient interfacial heat transfer coefficients in chill mold castings, J. Alloys Comp. 319 (2001) 174–186.
[10] J. Brimacombe, I. Samarasekera, J. Lait, Continuous casting heat flow, solidification and crack formation, Iron Steel Soc. AIME 2 (1984) 26.
[11] C.A. Santos, J.A. Spim, A. Garcia, Modeling of solidification in twin-roll strip casting, J. Mater. Proc. Technol. 102 (2000) 33–39.
[12] J.A. Brooks, M.I. Baskes, F.A. Greulich, Solidification modeling and solid-state transformations in high-energy density stainless-steel welds, Metall. Trans. A 22A (1991) 91–926.
[13] J. Spim, A. Garcia, Numerical analysis of solidification of complex shaped bodies: coupling of mesh elements of different geometries, Mater. Sci. Eng. A: Struct. 277 (1/2) (2000) 198–205.
[14] J.V. Beck, Combined parameter and function estimation in heat transfer with application to contact conductance, Trans. ASME 110 (11) (1988) 1046.
[15] J.V. Beck, Nonlinear estimation applied to the nonlinear inverse heat conduction problem, Int. J. Heat Mass Transfer 13 (1970) 703–716.
[16] M. Krishnan, D.G.R. Sharma, Determination of the interfacial heat transfer coefficient h in the unidirectional heat flow by Beck's non linear estimation procedure, Int. Commun. Heat Mass Transfer 23 (2) (1996) 203–214.
[17] T.S.P. Kumar, K.N. Prabhu, Heat-flux transients at the casting chill interface during solidification of aluminum base alloys, Metall. Trans. B 22 (1991) 717–727.
[18] K. Ho, R. Pehlke, Metal–mold interfacial heat transfer, Metall. Trans. B 16 (1985) 585–594.
[19] Y. Kim, B. Farouk, J. Keverian, A mathematical model for thermal analysis of thin strip casting of low carbon steel, J. Eng. Ind. 113 (1991) 53–58.

[20] T.P. Battle, R.D. Pehlke, Equilibrium partition coefficients in iron based alloys, Metall. Trans. B 20 (1989) 149–160.
[21] H.K.D.H. Bhadeshia, S.A. David, J.M. Vitek, Solidification sequences in stainless-steel dissimilar alloy welds, Mater. Sci. Technol. 7 (1991) 50–61.
[22] Metals Handbook, American Society for Metals, OH, 1973, p. 8.
[23] C. Siqueira, N. Cheung, A. Garcia, Solidification thermal parameters affecting the columnar to equiaxed transition, Metall. Trans. A 33 (7) (2002) 2107–2118.
[24] W. Loser, S. Thiem, M. Jurish, Solidification modeling of microstructures in near-net-shape casting of steels, Mater. Sci. Eng. A 173 (1993) 323–326.